Journal of Colloid and Interface Science **249,** 359–365 (2002)
doi:10.1006/jcis.2002.8268, available online at http://www.idealibrary.com on IDEAL®

Formation and Characterization of High Surface Area Thermally Stabilized Titania/Silica Composite Materials via Hydrolysis of Titanium(IV) *tetra*-Isopropoxide in Sols of Spherical Silica Particles

Kamal M. S. Khalil,*,[1] Ahmed A. Elsamahy,† and Mohamed S. Elanany†

*Chemistry Department, Faculty of Science, UAE University, P.O.B. 17551, Al-Ain, United Arab Emirates; and †Chemistry Department, Faculty of Science, South Valley University, P.O.B. 82524, Sohag, Egypt

Received March 15, 2001; accepted January 31, 2002; published online April 10, 2002

A direct synthetic route leading to titania particles dispersed on nonporous spherical silica particles has been investigated; 5, 10, and 20% (w/w) titania/silica sols mixtures were achieved via hydrolyzation of titanium *tetra*-isopropoxide solution in the mother liquor of a freshly prepared sol of spherical silica particles (Stöber particles). Titania/silica materials were produced by subsequent drying and calcination of the xerogels so obtained for 3 h at 400 and 600°C. The materials were investigated by means of thermal analyses (TGA and DSC), FT-IR, N_2 gas adsorption–desorption, powder X-ray diffraction (XRD), and transmission electron microscopy (TEM). In spite of the low surface area (13.1 m^2/g) of the pure spherical silica particles calcined at 400°C, high surface area and mesoporous texture titania/silica materials were obtained (e.g., S_{BET} ca. 293 m^2/g for the 10% titania/silica calcined at 400°C). Moreover, the materials were shown to be amorphous toward XRD up to 600°C, while reasonable surface areas were preserved. It has been concluded that dispersion of titania particles onto the surface of the nonporous spherical silica particles increase their roughness, therefore leading to composite materials of less firm packing and mesoporosity.

Key Words: **titania/silica; TiO_2/SiO_2; TEM; surface area; thermal stability.**

1. INTRODUCTION

The titania–silica system represents a prospective class of materials that have recently been used as catalysts and supporting materials (1–5), protective coating (6, 7), antireflectio coatings (8, 9), glass materials of low thermal expansion coefficient (8, 9), and paper whiteners (10). However, in spite of the vast number of studies regarding TiO_2–SiO_2 mixed oxide materials (chemically bonded), titania/silica-supported oxides (physically mixed) have been less investigated. In fact, titania/silica has been considered as an advanced support to replace pure TiO_2 support, which normally has a lower surface area and sinters more easily than supports like silica or alumina (11, 12). Moreover, applying of TiO_2 onto silica offers a way of obtaining a titania surface with high, thermally stable surface area and good mechanical properties (12).

However, properties such as surface area, porosity, and thermal stability of the supporting materials are largely determined by the precursors and processing method (13–15). Therefore, different synthetic approaches have been developed to prepare titania/silica-supported oxides of modifie structural and textural properties. A grafting procedure (16) via chemisorption of $TiCl_4$ onto mesoporous silica gel was performed in the dry helium fl w at 200 and 400°C. This was followed by the hydrolysis of the residual bonds of Ti–Cl (which is accompanied by hydrolysis of bridges Si–O–Ti) (16). Pore size distribution of titania/silica gel was found to depend on the TiO_2 concentration and the temperature of titania synthesis. Porous titania/silica gel materials have been synthesized (17) by using vapor deposition (CVD) of titania via repeated reactions of $TiCl_4$ with the surface and subsequent hydrolysis. Accordingly, TiO_2 was covering the silica gel surface in a nonuniform layer, where small particles embedded in pores and larger particles formed at the outer surface of silica globules. Therefore, porosity and fractality of samples decrease with increasing TiO_2. However, Hsu *et al*. (10) obtained titania coating onto silica dispersions by the addition of $TiOSO_4$ in 1 M H_2SO_4. In addition, titania/silica supports suitable for V_2O_5 supporting were prepared (12) via the addition of $TiCl_3$ to a suspension of nonporous silica followed by homogenous precipitation of hydrous Ti(III) oxide onto silica. Subsequent heat treatment at 550°C allowed the preparation of TiO_2 dispersed on the silica surface.

Recently, a new approach has been motivated in light of the evidence that sols of colloidal oxides can play a critical role as precursors of unique supported oxide materials (18). The present work investigates titania/silica materials formed via their sol interaction. The formation was achieved via basic hydrolysis of silicon tetraethoxide, TEOS, into spherical sol particles (prepared by the Stöber method) (19) and the subsequent

[1] To whom correspondence should be addressed. Fax: 00971-3-7671291. E-mail: kamalk@uaeu.ac.ae. Permanent address: Chemistry Department, Faculty of Science, South Valley University, P.O.B. 82524, Sohag, Egypt.

0021-9797/02 $35.00

addition of titanium(IV) *tetra*-isopropoxide, TTIP, to the mother liquor of the formed sol solution. The goal of the present procedure is to offer high surface area titania/silica materials with high textural and thermal stability.

2. EXPERIMENTAL

2.1. Materials

The materials consist of tetraethyl orthosilicate, 98% $Si(OC_2H_5)_4$, TEOS, liquid, product of Sigma-Aldrich Co., Ltd., Germany; titanium *tetra*-isopropoxide, $Ti[OCH(CH_3)_2]_4$, TTIP, liquid, product of Aldrich Chemical Co., Ltd., England; ammonia solution, (25% NH_3) sp. gr. 0.91, product of BDH Limited, England; isopropanol, $CH_3CHOHCH_3$, product of Merck, Germany; and ethyl alcohol absolute, C_2H_5OH, (GPR) product of ADWIC, Egypt.

Preparation of the pure silica supports. In a 600-ml baker 207.0 ml of absolute alcohol and 19.0 ml of TEOS were added. The hydrolysis was accomplished by the addition of 155 ml of ammonia (within 1 min) with magnetic stirring (400 rpm). After a few minutes, turbidity started to appear and the solution turned opaque white due to dense silica sol formation (Stöber particles). The sol was kept under stirring for 1.5 h. The resultant solution was aged for 1 week. The cake thus stilled was filtered off using Whatman filter paper. The collected material was left for drying overnight at 60°C and allowed for further drying at 100°C for 24 h. The material thus produced was termed as "dried pure silica precursor." Portions of the dried precursor were calcined in a muffle furnace at 400 and 600°C for 3 h to prepare the test samples.

Preparation of 5–20 (w/w%) titania/silica materials. Supports of silica loaded with 5, 10, 15, and 20% titania were prepared by the following procedure. The hydrolysis of TEOS into silica sol particles proceeded as above. After 30 min, a calculated amount of titanium *tetra*-isopropoxide, TTIP (equivalent to the desired loading percentage), diluted in isopropanol (to the total volume of 50 ml) was added (through 1 min) to the silica sol solution at a stirring rate of 400 rpm. The solutions were kept under stirring for 1.0 h more. The solutions were aged for 1 week without covering in a fume cupboard. Then, the coagulated cake thus obtained was collected and dried as for the pure silica precursor. The materials thus obtained are termed as "dried precursors". Test samples were obtained by the calcination of portions of the dried precursors in a muffle furnace for 3 h at 400 and 600°C.

2.2. Investigation Techniques

Thermal analysis (TGA and DSC). Analyses were carried out utilizing a Thermal Analyst 2000 TA instrument (USA) controlling a 2050 thermogravimetric (TG) analyzer and a 2010 differential scanning calorimeter (DSC). A ceramic sample boat was used for TG runs. Samples weighing 10.0 ± 0.1 mg were heated up to 900°C at 10°C/min and in a stream (30 ml/min) of nitrogen atmosphere. For DSC measurement, open aluminum sample pans were used. Samples weighing 5.0 ± 0.1 mg were heated up to 500°C at 10°C/min in a dynamic atmosphere of nitrogen (30 ml/min).

Fourier transform infrared (FTIR) spectroscopy. FTIR spectra for the samples of investigation were carried out using a Shimadzu FTIR-8101 Fourier transform infrared spectrophotometer, Shimadzu (Japan) in the range 4000–400 cm^{-1}, the number of scans was 40, and resolution was 4 cm^{-1}.

X-ray diffractometry. X-ray powder diffractograms of the different samples and their calcination products at different temperatures were measured on a Siemens D 5000 powder X-ray diffractometer (Germany). Diffraction patterns were recorded with Ni-filtered Cu$K\alpha$ radiation ($\lambda = 1.5418$ Å). An on-line data acquisition and handling system (Diffract Software, Siemens) was used for phase identification purposes (20).

Transmission electron microscopy (TEM). TEM micrographs were obtained, using a model JEM-1010 Jeol microscope (Japan). Test samples were prepared by ultrasonic dispersion of the solid in alcohol. A drop of the resulting suspension was doped onto a carbon-coated grid and allowed to dry at 60°C before testing.

Nitrogen gas adsorption. Nitrogen adsorption/desorption isotherms at 77K were measured using a model ASAP 2010 (Micromeritics Instrument Corporation, USA). Prior to measurement, all samples were outgassed for 2 h at 150°C to 0.1 Pa. The specific surface area, S_{BET}, was calculated applying the BET equation (21). Porosity distribution (>2 up to >100 nm) was generated by the DFT plus V1.00 (2010) software of the instrument indicated applying the original density function theory and slit pores shape model (22–24). Assessments of microporosity were made from *t*-plot constructions, using the Harkins–Jura correlation (25) for *t*-plot as a function of normalized pressure, p/p_o. Parameters were fitted to a low-area, nonporous silica. *t*-Plot surface areas were determined from slope analysis of the *t*-plots, similar to the reported data processing given by Handy *et al.* (26).

3. RESULTS AND DISCUSSION

3.1. TG and DSC Analyses

Total weight loss that was observed for the pure silica precursor upon heating from 25°C up to 900°C (Fig. 1) was 10.04%. However, increasing weight losses, which increase with the increase of TiO_2 contents, were recorded for the TiO_2/SiO_2 precursors, e.g., 14.39% for the 20% titania/silica precursor (see Table 1). The weight loss in a nitrogen atmosphere originated mainly from the desorption of physically sorbed water (and or solvents) and surface dehydroxylation (5). The differential thermogravimetric (DTG) profile obtained from the dried silica precursor showed two peaks (Fig. 1). The first was shown between 50 and 200°C and the second, which was weak and broad, was shown between 400 and 600°C. DTG profiles

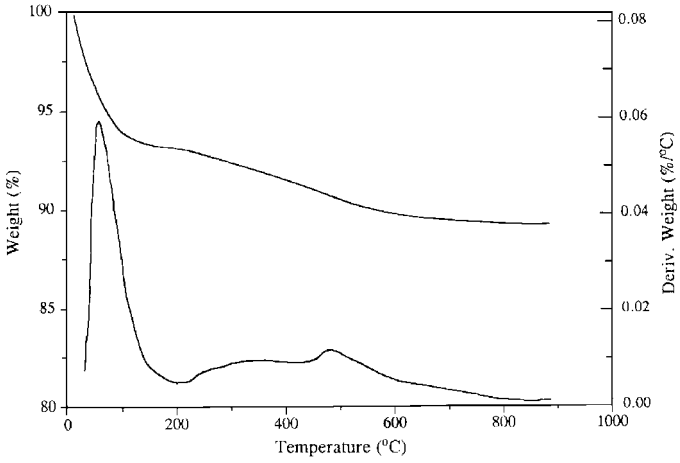

FIG. 1. TGA and DTG thermograms for the pure spherical silica precursor carried out in a nitrogen atmosphere.

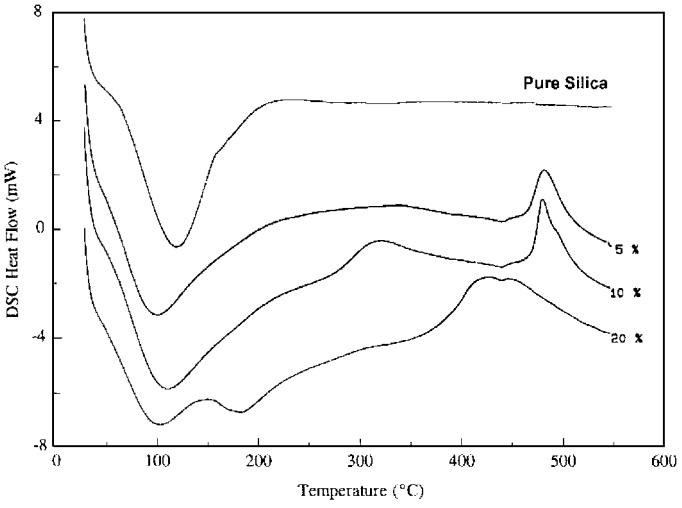

FIG. 2. DSC thermograms for the pure silica and titania/silica precursors containing 5, 10, and 20% of TiO_2 carried out in a nitrogen atmosphere.

obtained from the dried titania/silica precursors also showed two peaks. The first was shown between 50 and 200°C and the second was shown between 460 and 510°C, maximizing at ca. 485°C.

The differential scanning calorimetery (DSC) profiles obtained for a dried support precursor along with the pure silica (Fig. 2) showed two major peaks. The first, which was endothermic, maximizes near 100°C (whereas at 130°C for the pure silica precursors) in association with the first DTG peak, which was assigned to the removal of retained water and solvents. Enthalpies associated with this peak for the different precursors (see Table 1) showed a large decrease upon loading and/or increasing of TiO_2 contents.

The second peak shown by the DSC profiles for the titania/silica (but not for the pure silica precursor) was exothermic and maximized at 480°C in association with the second DTG peak. However, for the 20% titania/silica precursor a diffused peak that maximizes at 428–448°C was observed. Heat enthalpies associated with this peak were −28.0, −23.0, and −91.1 J/g for the precursor containing 5, 10, and 20% TiO_2, respectively. These values are rather smaller than the value (208.5 J/g) measured for a pure titania precursor test sample (at 430°C, due to transformation into anatase).

3.2. X-Ray Diffractometry

Powder diffractograms obtained for the different titania/silica materials calcined at 400 and 600°C product reveal their amorphous nature, no matter what the TiO_2 ratio and/or the calcination temperature was. Typical diffraction patterns obtained for the 20% titania/silica along with that for pure silica (both calcined at 600°C), as representatives, are shown in Fig. 3. XRD results indicated that no crystalline phases were formed upon calcination up to 600°C whereas pure titania precursor is known to crystallize into anatase upon calcination at 400°C (15).

3.3. FTIR Spectra

FTIR spectra of the pure silica precursor dried at 100°C (Fig. 4) agrees with those for fully hydrolyzed TEOS (silica gel) (27, 28). With increasing calcination temperature to 400 and 600°C (Fig. 4), all the peaks become weaker and weaker. Therefore, the 953-cm^{-1} peak assigned to Si–OH stretching was disappeared in both cases. The 3437 and 1640 cm^{-1} peaks assigned for the stretching vibration of the OH group and

TABLE 1
TGA and DSC Results for the Pure Silica and Different Titania/Silica Precursors

Precursor	TGA weight loss %, RT-900°C	DSC 1st peak			DSC 2nd peak		
		Range, °C	T_{Max}, °C	Heat, J/g	Range, °C	T_{Max}, °C	Heat, J/g
Pure silica	10.04	65–230	130	+258	No peak was observed		
5% titania	11.64	59–220	99	+121	464–521	483	−28.9
10% titania	12.06	61–220	109	+123	471–521	482	−23.0
20% titania	14.39	60–220	103 and 182	+96	360–540	428 and 448	−91.9
Pure titania	—	No peak was observed			383–463	430	−208.5

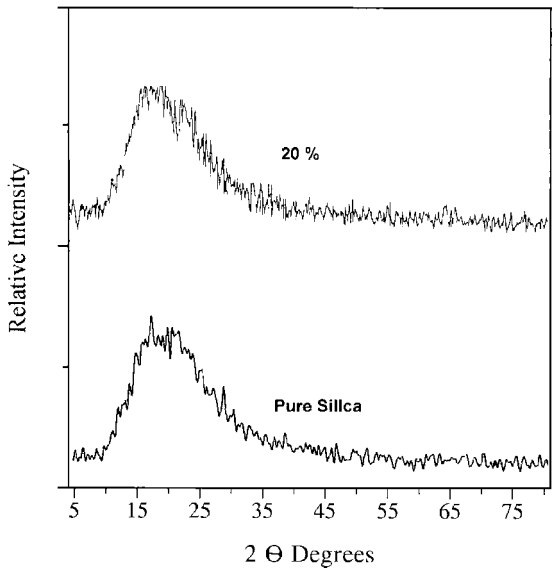

FIG. 3. Powder XRD patterns for pure silica material and 20% titania/silica material, both calcined at 600°C.

molecular H_2O, respectively, were effectively removed after calcination at 600°C.

FTIR spectra for the different titania/silica materials calcined at 100, 400, and 600°C (e.g., see Fig. 5, for the 600°C calcined

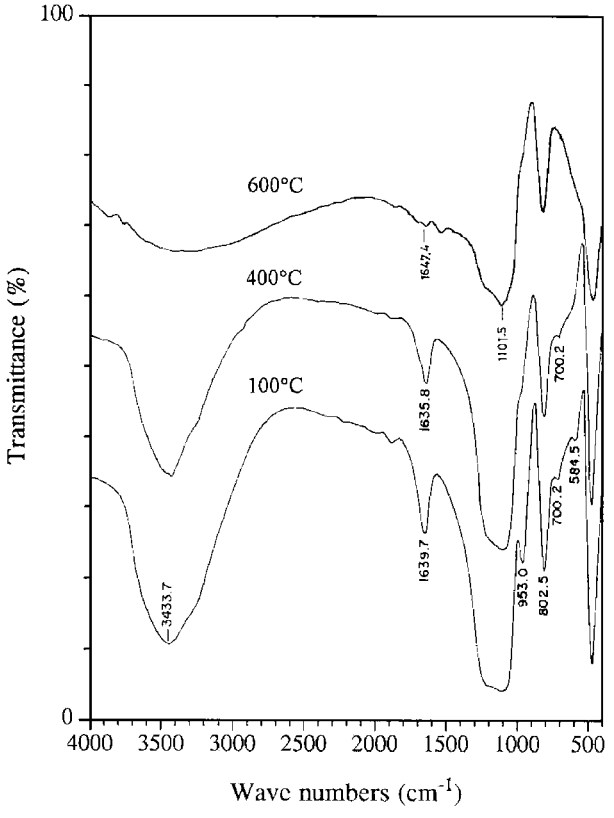

FIG. 4. FTIR spectra for pure silica precursor thermally treated at 100, 400, and 600°C.

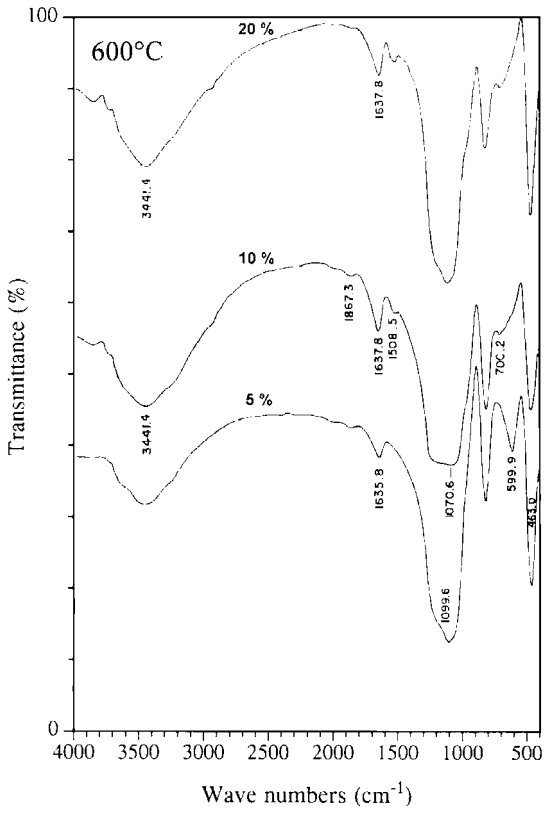

FIG. 5. FTIR spectra for 5, 10, and 20% titania/silica materials calcined at 600°C.

materials) showed features that are similar to the pure silica. In light of the major vibrations reported for similar systems (2, 5), the 464-cm^{-1} peak is assigned for Si–O–Si bending modes, the 800-cm^{-1} peak is assigned for symmetric ν_s(Si–O–Si) stretching vibration, and the 1098-cm^{-1} peak is assigned for asymmetric ν_{as}(Si–O–Si) stretching vibration. In addition, minor features were observed in the region 1400–1550 cm^{-1}; these can be assigned to the different mode of retained NH_3 or NH_4^+ species on the surface of the materials.

3.4. Electron Microscopy

Figures 6a and 6b show typical micrographs for the pure silica calcined at 400 and 600°C, respectively. TEM for the 400°C calcined product show that the pure silica particles are spherical in shape and nearly equal in size (400–600 nm). The micrograph also reveals that the particles are closely packed together. Coordination number as high as 6 (other particles) can be observed for many particles. This morphology led to a closely packed structure with low pore volume, as conf rmed by N_2 gas adsorption results; see below. The micrograph for the 600°C calcined pure silica material (Fig. 6b) showed similar morphology to the 400°C calcined material. Nevertheless, increasing particle coalescence can be observed at particle-to-particle neck points. This indicates the progress of the sintering process, which leads to loss of surface area and porosity (see S_{BET} results below).

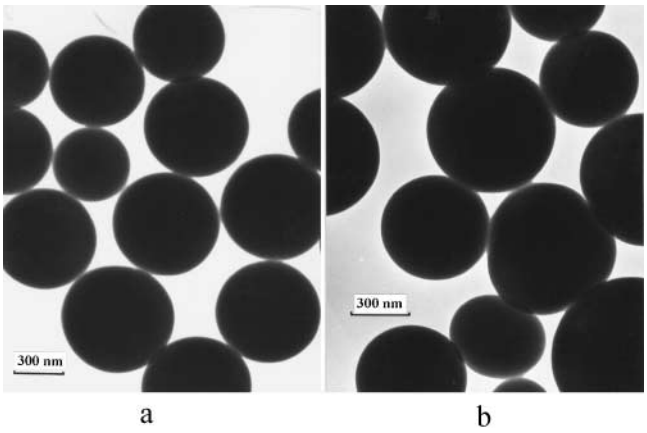

FIG. 6. TEM micrographs for pure silica calcined at 400°C (a) and at 600°C (b).

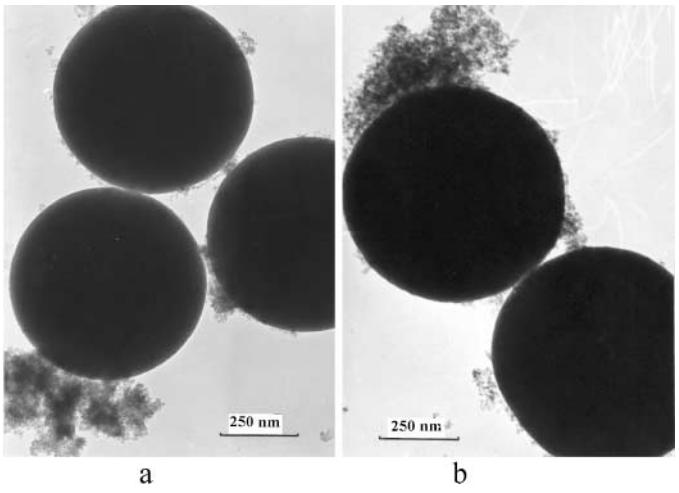

FIG. 8. TEM micrographs for 10% titaina/silica (a) and 20% titania/silica (b) materials calcined at 600°C.

Micrographs for the 10 and 20% titania/silica materials calcined at 400°C are shown in Figs. 7a and 7b, respectively. TEM reveals that the materials consist of a composite of two distinct phases, actually a spherical silica particles matrix (similar in shape and size to that observed for pure silica material) and titania particles impeded between or on the surface of the silica particles. Clearly, the presence of titania particles increases the roughness of the spherical silica particles and this effect increases with the increase of the TiO_2 ratio (compare Fig. 7a with Fig. 7b). However, some titania particles were aggregating between the spherical silica particles; this also was increased with the increasing of titania ratio.

TEM micrographs for the 10 and 20% titania/silica materials calcined at 600°C (Figs. 8a and 8b, respectively) are largely similar to those observed for the 400°C calcined materials, but titania aggregates were slightly larger in size. Moreover, less coalescence was observed between silica particles at particle-to-particle neck points (in comparison with the case of the pure silica particles calcined at the same temperature). This indicates that the presence of titania particles retards the sintering process and leads to the texture stability of the materials.

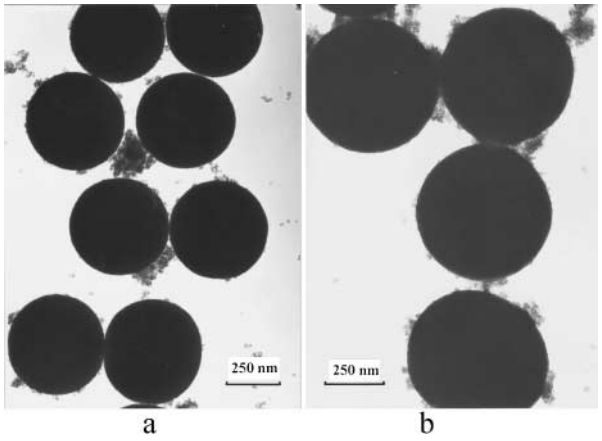

FIG. 7. TEM micrographs for 10% titania/silica (a) and 20% titania/silica (b) materials calcined at 400°C.

3.5. Texture Assessment by Nitrogen Adsorption Isotherms

Textural properties for the pure and different titania/silica supports are cited in Table 2, along with some other results reported for the pure TiO_2 prepared by basic hydrolysis (15), or controlled hydrolysis (29), and Z(TS-1) zeolite (5) for comparison. Nitrogen adsorption/desorption isotherms for the pure silica materials

TABLE 2

Textural Properties of the Prepared Supporting Materials Calcined in Air at Different Temperatures along with Some Other Supports Given for Comparison

Support	Calc. (°C)	Isotherm type	Hystersis loop	S_{BET} (m^2/g)	S_t	$S_{Ext.}$	d_{max} (nm)
Pure	400	II	no	13.1	5.7	7.4	52
5%	400	IV(+II)	H1	178.1	130.4	47.7	26
10%	400	IV	H1	293.3	202.2	91.1	19
20%	400	IV	H1	215.3	86.6	128.7	32
Pure	600	II	No	9.5	5.3	4.2	54
5%	600	IV	H1	45.8	8.3	37.5	29
10%	600	IV	H1	65.8	5.2	60.6	20
20%	600	IV	H1	110.5	3.6	106.9	30
Pure TiO_2[a]	400	IV	H2	67	—	—	—
Pure TiO_2[b]	400	IV	H2	131.9	—	—	10
Pure TiO_2[b]	600	IV	H2	58.5	—	—	10
Z (TS-1)[c]	550			417	306	111	45

[a] Pure TiO_2 prepared by basic hydrolysis of titanium *tetra*-isopropoxide; mixing molar ratios were 1.0 : 1.0 : 3.1 alkoxy group : ammonia : water, Ref. (15).

[b] Pure spherical TiO_2 prepared by hydrolysis of titanium *tetra*-isopropoxide in *n*-heptane, Ref. (29).

[c] Zeolite TS-1 (3.1 wt% TiO_2), Ref. (5).

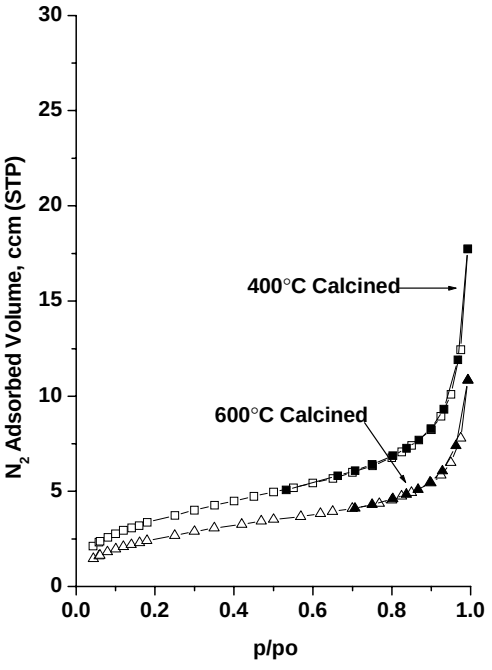

FIG. 9. Nitrogen adsorption/desorption isotherms obtained from pure silica materials calcined at 400 and 600°C.

calcined at 400 and 600°C are shown in Fig. 9. The isotherms showed a type-II isotherm without any obvious hysteresis loops according to IUPAC classif cation. S_{BET} surface areas were 13.1 and 9.5 m^2/g, and the corresponding S_t (micropore surface area estimated from the appropriate *t*-plot analysis) were 5.7 and 5.3 m^2/g for the pure silica materials calcined at 400 and 600°C, respectively. Weak porosity distributions were obtained in the range 40–100 nm with maxima at 52 and 54 for the 400 and 600°C calcined materials, respectively.

Titania/silica materials calcined at 400°C showed type-IV isotherms (with little contribution from type-II) and H1-type hysteresis. Titania/silica materials calcined at 600°C (shown in Fig. 10) showed typical type-IV isotherms, with type H1 hysteresis loops that are often obtained with materials consisting of agglomerates or compacts of approximately uniform spheres in a fairly regular array (23).

Specif c surface area, S_{BET}, of titania/silica materials calcined at 400°C are shown in Table 2. The table shows that titania supported on silica produced an effective increase of the S_{BET} values up to 293.3 $m^2\ g^{-1}$ as the titania content increased to 10%. A subsequent increase of the titania content slightly decreases the S_{BET} values to 215.3 $m^2\ g^{-1}$ for the 20% TiO_2 containing material. The S_t values increase from 130.4 to 202.2 for the 5 and 10% TiO_2 containing materials. Then, a subsequent increase of the titania content decreases the values to 86.6 $m^2\ g^{-1}$ for the 20% TiO_2 containing material. However, when the S_t values were subtracted from the corresponding S_{BET} values, values termed as external surface area, S_{Ext}, are obtained (see Table 2). The S_{Ext} values, which are related to the surface of pores > micropore dimensions, i.e., meso- and macropores, showed gradual development (from 47.7 to 91.1 to 128.7 m^2/g^{-1}) with the increase of titania contents (from 5 to 10 to 20%, respectively).

For the 600°C calcined materials, S_{BET} values were increasing (from 45.8 to 65.8 to 110.5 $m^2\ g^{-1}$), whereas S_t values were decreasing (from 8.3 to 5.2 to 3.6 $m^2\ g^{-1}$) with the increasing TiO_2 content from 5 to 10 to 20%, respectively. The S_{Ext} values, obtained by subtraction of S_t from S_{BET} as above, were 37.5, 60.6, and 106.9 $m^2\ g^{-1}$ for 5, 10, and 20%, respectively.

Pore size distribution, PSD, curves obtained for the materials calcined at 400°C showed enhanced distributions in the range <10 to ~70 nm, which were at 26, 19, and 32 nm for the 5, 10, and 20% titania/silica, respectively. Similar PSDs were observed for the 600°C calcined materials with maxima at 29, 20, and 30 nm for the 5, 10, and 20% titania/silica, respectively. These results indicate the improvement of porosity upon increasing titania ratio.

3.6. Formation and Stabilization of the Porous Texture

The present method examined the formation of so-called microengineered catalytic structure via mixing of two distinct sols, namely, titania and silica sol particles (18). Previous investigation showed that basic hydrolysis of TTIP in a protic or aprotic solvent produced high surface area titania particles of nanaosize particles (15). However, as a matter of fact, high surface area titania particles are subject to sintering and loss of surface area at higher temperature due to phase transformation (see Table 2 for the pure TiO_2^b calcined at 400 and 600°C) (29). Accordingly,

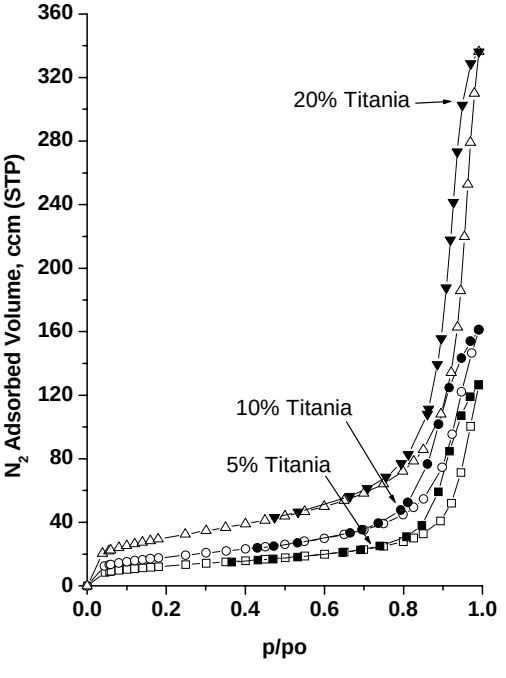

FIG. 10. Nitrogen adsorption/desorption isotherms obtained from 5, 10, and 20 titania/silica materials calcined at 600°C.

the S_{BET} was decreased from 131.9 to 58.5 m^2/g upon increasing of the calcination temperature from 400 to 600°C. However, in the present work higher surface areas were observed for the materials containing ≤20% titania. For example, the 20% titania material calcined at 400 and 600°C showed S_{BET} values of 215.3 and 110.5, respectively. These values are higher than the values reported for the corresponding pure titania powder (15, 29). Moreover, if the external surface area is to be considered (see Table 2), the S_{EXT} value 106.9 $m^2\ g^{-1}$ for 20% titania material calcined at 600°C is very comparative with the value reported for the reference zeolite, Z(TS-1), which amounts to 111 for the sample calcined at 550°C.

Thus, the consequence of the interaction between titania particles and silica sols on the texture properties of the produced composite materials can be explained in terms of the increasing voids created between silica particles due to titania particles segregation at the contact point between silica spheres. This is justif ed in terms of the gradual increasing of TGA weight losses with the increase of TiO_2 ratio. The decrease of the heat enthalpies of the endothermic DSC peak may also ref ect the facile evaporation (of water and/or solvents) due to the increased porosity created by segregation of titania particles in the xerogel precursors. The thermal event characterized by the exothermic DSC peak at 480°C (with heat enthalpies less than the requirement for the crystallization of titania) was not accompanied by the formation of any crystalline products upon calcination at 600°C (XRD results). Thus, this event may be assigned to the aggregation of the rather small titania particles into bigger ones in a process preceding the crystallization process of titania particles (28). The reduction of both S_{BET} and S_t values (specially, the latter) upon increasing calcination temperature from 400 to 600°C supports the presence of such aggregation processes of titania particles, which are supposed to lead to less roughened particles. Therefore, the produced texture prevents crystallization of titania particles even upon calcination at 600°C due to their presence in the voids between silica particles. The crystallization prevention may be due to the presence of a highly hydroxylated surface of trapped porosity, which exhibits dehydroxylation up to 900°C. Moreover, the presence of titania particles on the spherical surface of the silica particles prevent their coalescence.

4. CONCLUSIONS

The above results showed that dispersion of titania particles in a mattress of spherical silica particles was achieved via a simple "one-pot" processing. All the materials formed were noncrystalline and thermally stable. These materials take advantage of the highly dense silica particles (Stöber particles) of great mechanical stability and overcome their disadvantage of low surface area and inert surface via dispersion of reactive titania phase. Therefore, dispersion of titania particles increased the surface area and improved the porosity of the spherical silica particles matrix. In comparison, some other reported method for titania grafting leads to loss of surface area and blocking of porosity.

REFERENCES

1. Watson, R. B., and Ozkan, U. S., *J. Catal.* **191,** 12 (2000).
2. Gao, X., and Wachs, I. E., *Catal. Today* **51,** 233 (1999).
3. Davis, R. J., and Liu, Z., *Chem. Mater.* **9,** 2311 (1997).
4. Liu, Z., and Davis, R., *J. Phys. Chem.* **98,** 1253 (1994).
5. Dutoit, D. C. M., Schneider, M., and Baiker, A., *J. Catal.* **153,** 165 (1995).
6. Atik, M., and Zarzycki, J., *J. Mater. Lett.* **13,** 1301 (1994).
7. Atic, M., Neto, P. D. L., Aergerter, M. A., and Avaco, L. A., *J. Appl. Electrochem.* **25,** 142 (1995).
8. Brinker, C. J., and Scherer, G. W., "Sol-Gel Science, The Physics and Chemistry of Sol-Gel Processing". Academic Press, New York/London, 1989.
9. Yu-Zhang, K., Boisjolly, G., Rivory, J., Kilian, L., and Colliex, C., *Thin Solid Films* **253,** 299 (1994).
10. Hsu, W. P., Yu, R., and Matijevic, E., *J. Colloid Interface Sci.* **156,** 56 (1993).
11. Reiche, M. A., Ortelli, E., and Baiker, A., *Appl. Catal. B* **23,** 187 (1999).
12. Quaranta, N. E., Soria, J., Cortés Corberán, V., and Fierro, J. L. G., *J. Catal.* **171,** 1 (1997).
13. Khalil, K. M. S., *J. Catal.* **178,** 198 (1998).
14. Khalil, K. M. S., Baird, T., Zaki, M. I., El-Samahy, A. A., and Awad, A. M., *Colloids Surf. A* **132,** 31 (1988).
15. Khalil, K. M. S., and Zaki, M. I., *Powder Technol.* **92,** 233 (1997).
16. Gun Ko, V. M., Villieras, F., Leboda, R., Marciniak, M., Charmas, B., and Skubiszewska-Zieba, J, *J. Colloid Interface Sci.* **230,** 320 (2000).
17. Leboda, R., Gun Ko, V. M., Marciniak, M., Malygin, A. A., Malkin, A. A., Grzegorczyk, W., Trznadel, B. J., Pakhlov, E. M., and Voronin, E. F., *J. Colloid Interface Sci.* **218,** 23 (1999).
18. Murrell, L. L., *Catal. Today* **35,** 225 (1997).
19. Stöber, W., Fink, A., and Bohn, E., *J. Colloid Interface Sci.* **26,** 62 (1968).
20. JCPDS, International Center for Diffraction Data, CD, 1996.
21. Brunauer, B., Emmett, P. H., and Teller, E., *J. Am. Chem. Soc.* **60,** 309 (1938).
22. Gregg, S. J., and Sing, K. S. W., "Adsorption, Surface Area and Porosity," 2nd ed, Academic Press, New York, 1982.
23. Refer to "Micromertics DFT plus, Operator's Manual" V1.00, Micrometrics Instrument Corp., 1996. Tarazona, P., *Phys. Rev.* **31,** 2672 (1985). Tarazona, P., Marconi, U. M. B., and Evans, R., *Mol. Phys.* **60,** 543 (1987).
24. International Union of Pure and Applied Chemistry, IUPAC, *Pure Appl. Chem.* **57,** 603 (1985).
25. Harkins, W. D., and Jura, G., *J. Chem. Phys.* **11,** 431 (1943).
26. Handy, B. E., Maciejewski, M., Baiker, A., and Wokaun, A., *J. Mater. Chem.* **2,** 833 (1992).
27. Brinker, C. J., and Scherer, G. W., *in* "Sol-Gel Science, The Physics and Chemistry of Sol-Gel Processing," pp. 581–582. Academic Press, New York/London, 1989, and references therein.
28. Duran, A., Fernandez-Navarro, J. M., Casasriego, P., and Joglar, A., *J. Non-Cryst. Solids* **82,** 69 (1986).
29. Khalil, K. M. S., and Zaki, M. I., *Powder Technol.* **120,** 256 (2001).